PNAS Nexus, 2024, 3, 1–10
https://doi.org/10.1093/pnasnexus/pgad428
Advance access publication 14 December 2023
Research Report

Sudden adiabaticity signals reentrant bulk superconductivity in UTe_2

Rico Schönemann [a,*], Priscila F. S. Rosa [b], Sean M. Thomas [b], You Lai [a], Doan N. Nguyen [a], John Singleton [a], Eric L. Brosha [c], Ross D. McDonald [a], Vivien Zapf [a], Boris Maiorov [a] and Marcelo Jaime [a,*,1]

[a]MPA-MAGLAB, Los Alamos National Laboratory, Los Alamos, NM 87545, USA
[b]MPA-Q, Los Alamos National Laboratory, Los Alamos, NM 87545, USA
[c]MPA-11, Los Alamos National Laboratory, Los Alamos, NM 87545, USA
*To whom correspondence should be addressed: Email: rschoenemann@lanl.gov (R.S.); Email: marcelo.jaime@ptb.de (M.J.)
[1]Present Address: Physikalisch Technische Bundesanstalt, Braunschweig, Germany
Edited By: J.C. Davis

Abstract

There has been a recent surge of interest in UTe_2 due to its unconventional magnetic field (H)-reinforced spin-triplet superconducting phases persisting at fields far above the simple Pauli limit for $H \parallel [010]$. Magnetic fields in excess of 35 T then induce a field-polarized magnetic state via a first-order-like phase transition. More controversially, for field orientations close to $H \parallel [011]$ and above 40 T, electrical resistivity measurements suggest that a further superconducting state may exist. However, no Meissner effect or thermodynamic evidence exists to date for this phase making it difficult to exclude alternative scenarios. In this paper, we describe a study using thermal, electrical, and magnetic probes in magnetic fields of up to 55 T applied between the [010] (b) and [001] (c) directions. Our MHz conductivity data reveal the field-induced state of low or vanishing electrical resistance; our simultaneous magnetocaloric effect measurements (i.e. changes in sample temperature due to changing magnetic field) show the first definitive evidence for adiabaticity and thermal behavior characteristic of bulk field-induced superconductivity.

Keywords: magnetocaloric effect, proximity detector oscillator, high pulsed magnetic fields, unconventional superconductivity

Significance Statement

A field-induced state in UTe_2 was previously studied via electrical and magnetic properties and interpreted as superconductivity, yet thermodynamic evidence is lacking. Our magnetocaloric effect measurements provide strong thermodynamic evidence for a bulk state characterized by gapped excitations that carry charge but not heat. We identify its bulk nature from reversible heating in pulsed magnetic fields and the sudden increase in thermal relaxation time constant or adiabaticity, taken together with high electrical conductivity, characteristics of superconducting pairs carrying no entropy. Our results advance the understanding of the nature of the field-induced state and constrain theoretical modeling.

Introduction

The recently discovered actinide superconductor UTe_2 has been predicted as a promising candidate for the realization of chiral spin-triplet superconductivity with equal-spin pairing. Support for this picture comes from its close proximity to magnetic order, its unusually large critical magnetic field (far exceeding the Pauli limit for a weakly coupled Bardeen-Cooper-Schrieffer [BCS]-type superconductor in the absence of spin–orbit coupling), as well as the observation of only a small change in the Knight shift below its superconducting transition temperature $T_c \approx 1.6$–2.1 K (1–9). UTe_2 crystallizes in a body-centered orthorhombic structure (*Immm*) (1). Unlike closely related orthorhombic UGe_2, URhGe, and UCoGe, for which superconductivity emerges within the ferromagnetically ordered state (7), no signs of superconductivity coexisting with magnetic order were observed in UTe_2 down to 25 mK (10, 11). Magnetic fluctuations are believed to play a major role in facilitating superconductivity in UTe_2 (7), yet the nature of the fluctuations is still a matter of contention. Indeed, while some experiments give evidence for ferromagnetic fluctuations (1), recent neutron scattering data show excitations at an antiferromagnetic wave-vector (12). Studies under hydrostatic pressure also support the presence of antiferromagnetic fluctuations (13, 14).

When a magnetic field is applied along the magnetically hard b-axis, a reinforcement of superconductivity is observed above 15 T, which is extended up to 35 T (8). At this field $\mu_0 H_m \approx 35$ T, a first-order metamagnetic transition into a field-polarized paramagnetic phase occurs below 8 K, leading to a jump of $0.5\mu_B$ in the magnetization and the termination of the superconducting state (2, 4, 15). A smaller anomaly around 6.5 T was also reported

Competing Interest: The authors declare no competing interest.
Received: July 12, 2023. **Accepted:** November 27, 2023

in magnetization data for $H \parallel [100]$ (15). It is likely that a Fermi-surface reconstruction, as well as a volume/valence change, accompanies the metamagnetic transition (16). Thermopower and Hall data show a change of the majority charge and heat carriers from electrons to holes with a step-like increase in the electrical resistivity (3). Based on the Hall data, the estimated carrier density for $H > H_m$ is around a factor of six lower than that for $H < H_m$ (17).

On rotating the magnetic field from $H \parallel [010]$ to $H \parallel [001]$, the metamagnetic transition at H_m shifts upwards in field. Interestingly, when the field lies in a narrow angular range around the [011] direction, i.e. ≈23.7° away from the [010] axis, transport measurements suggest that a state with an undetectable low resistance emerges within the field-polarized paramagnetic phase above H_m. This state has been interpreted as superconductivity (2, 7, 18, 19), see Fig. 1A; however, it is nearly impossible to distinguish a true zero-resistance state from a simpler very low resistance state, or if such state is filamentary or bulk in nature. Constructing a theoretical model for superconductivity in strongly correlated electron systems has proven to be a phenomenally complex task. Until its bulk nature is established, extrinsic effects such as local stoichiometry, strain, lattice defects, impurities, etc. cannot be ruled out; all bets to explain the phenomenon are off. Crucial bulk thermodynamic evidence is still rather scarce though. Indeed, thus far low-temperature thermodynamic measurements have focused on magnetic fields along the principal axes *a*, *b*, and *c*, yet none for $H \parallel [011]$ (8, 20).

Here, we report complementary proximity detector oscillator (PDO) (21, 22), magnetocaloric effect (MCE) (23, 24), and angular-dependent torque magnetometry measurements to 55 T that are eminently applicable in this context, as they provide together an unambiguous thermodynamic detection of phase transitions and were conducted in the pulsed magnetic fields required to observe the high-field phase. Our combined results show the first bulk evidence for a state characterized by extremely high electrical conductivity, reversible increase in temperature, and thermal decoupling from the bath, likely due to fully gaped bulk superconductivity.

Results

Figure 1A shows the phase diagram of UTe_2 for magnetic field magnitude and orientation ($H - \theta$); with the angle θ describing the field rotating from parallel to the crystallographic *b*-axis ($\theta = 0°$) toward the *c*-axis ($\theta = 90°$). The phase diagram is based on prior magnetization, electric, and thermal transport measurements (1–4, 7, 18); the points (solid triangles) surrounding the high-field phase SC_{FP} were taken from Ran et al. (2). Despite sample temperature *T* excursions of up to ≈1.0 K (described in detail below), far from equilibrium with the ^{3}He bath temperature (≈0.6 K), the field positions of both the high-field metamagnetic and low-field transition out of the SC_{PM} phase obtained from MHz conductivity data with our Proximity Detector Oscillator (PDO) and magnetocaloric effect (MCE) measurements are in good agreement with prior data. In the case of the metamagnetic transition, this is unsurprising as H_m is virtually temperature independent for $T < 4$ K (7). Fig. 1B shows the specific heat divided by temperature c_p/T vs. temperature for a single-crystal sample in the same batch as the one used for MCE measurements, attesting to the sample's high quality. Fig. 1C shows a schematic of the UTe_2 sample mounted for simultaneous MCE and PDO measurements in pulsed fields. Note that the 100-nm thick AuGe film used as a thermometer has insignificant mass and a large contact surface with the sample, resulting in strong thermal coupling. In Fig. 1D, the magnetic field H and d*H*/dt vs. time are shown for the pulsed magnet used in these measurements.

For a direct comparison between results obtained at different field angles, examples of sample temperature *T* vs. field curves for $\theta = 18°$ and $\theta = 33°$ are shown in Fig. 2A and B on top of data from simultaneous PDO measurements (Fig. 2C and D). Referring to the phase diagram (Fig. 1A), at sub-Kelvin temperatures and $\theta = 18°$, the up-sweep of a 55 T field pulse first traverses the low-field SC_{PM} phase, then a metallic (paramagnetic, nonsuperconducting) phase followed by the metamagnetic transition at H_m before finally entering the field-polarized (FP) high-resistance phase. In contrast, at $\theta = 33°$, a similar pulse goes through the SC_{PM} phase, the metallic phase, and the metamagnetic transition (shifted to higher fields), where it enters the SC_{FP} phase. As we see, these different paths across the phase diagram result in different thermal responses.

Turning first to the MCE data at $\theta = 18°$ (Fig. 2A), as *H* initially rises (black curve) there is a steep increase in *T* from the ^{3}He bath temperature (≈0.6 K) to ≈1.1 K. This heating is attributable to an avalanche-like, dissipative vortex movement in the superconducting SC_{PM} phase, a phenomenon frequently seen in pulsed-field measurements of more conventional superconductors, e.g. Smylie et al. (25). Thereafter, *T* relaxes toward the bath temperature until a sharp step upwards denotes the first-order phase transition at H_m. Once in the FP state, *T* again relaxes for the rest of the up-sweep and during the start of the down-sweep (red curve). However, at H_m on the down-sweep there is another increase in *T*, followed by further relaxation down to around 15 T; below ≈13 T, there is an increase in *T*, likely due to a combination of SC gap opening and dissipative vortex motion as the removed field enables the SC_{PM} phase. Note that the down-sweep of *H* is much slower than the up-sweep, allowing more time for heat generated to dissipate (25). The most significant results for $\theta = 18°$ are (i) the irreversible processes that cause heating at the metamagnetic transition regardless of field-change direction, which dominates the thermodynamics, (ii) the thermalization (cooling off) of the sample in the high-field/high-resistance FP state. Here, the field changes do not cause eddy-current heating, and thermal coupling to the bath dominates the sample thermal response. (iii) Irreversible and reversible processes associated with the low-field SC_{PM} phase.

The simultaneous PDO data at $\theta = 18°$ (Fig. 2C) reflect these *T* changes. As the field increases (black curve), there is a sharp fall in *f* (increase in 1/*f*) at about 15 T, indicating the SC_{PM} to paramagnetic metal transition. The sample exits this state at $\mu_0 H_m \approx 38$ T. Once in the nonsuperconducting FP phase, changes Δf in the PDO frequency are dominated by changes in the sample skin-depth (closely related to the sample electrical resistivity)[a] (2, 21, 22). At H_m, ρ is known to exhibit a sharp increase (2), leading to a downward step in *f* (upturn in 1/*f*). Above H_m, the normal-state resistivity of UTe_2 is rather *T* independent in the range 0.6–2 K (2); hence, despite the varying *T* seen in the MCE data, the PDO frequency on the down-sweep of the field (red curve) overlies the up-sweep data. Below H_m, a step upwards (marked by an arrow) shows the transition back to the SC_{PM} phase; as *T* is lower on the down-sweep (Fig. 2A), this latter feature occurs at a slightly higher field than the corresponding feature in the up-sweep.

The MCE and PDO data for $\theta = 33°$ (Fig. 2B and D), below about 15 T, behave in a similar way to their counterparts at $\theta = 18°$. The PDO signal above 15 T at $\theta = 33°$ decreases roughly linearly, reflecting the increasing normal-state magnetoresistance. The biggest contrast for $\theta = 33°$ occurs on crossing H_m. The PDO data shows a sharp increase in frequency, result of a reduced inductance, indicating either a drastic reduction in skin-depth or a change into a new phase that expels the magnetic field. A

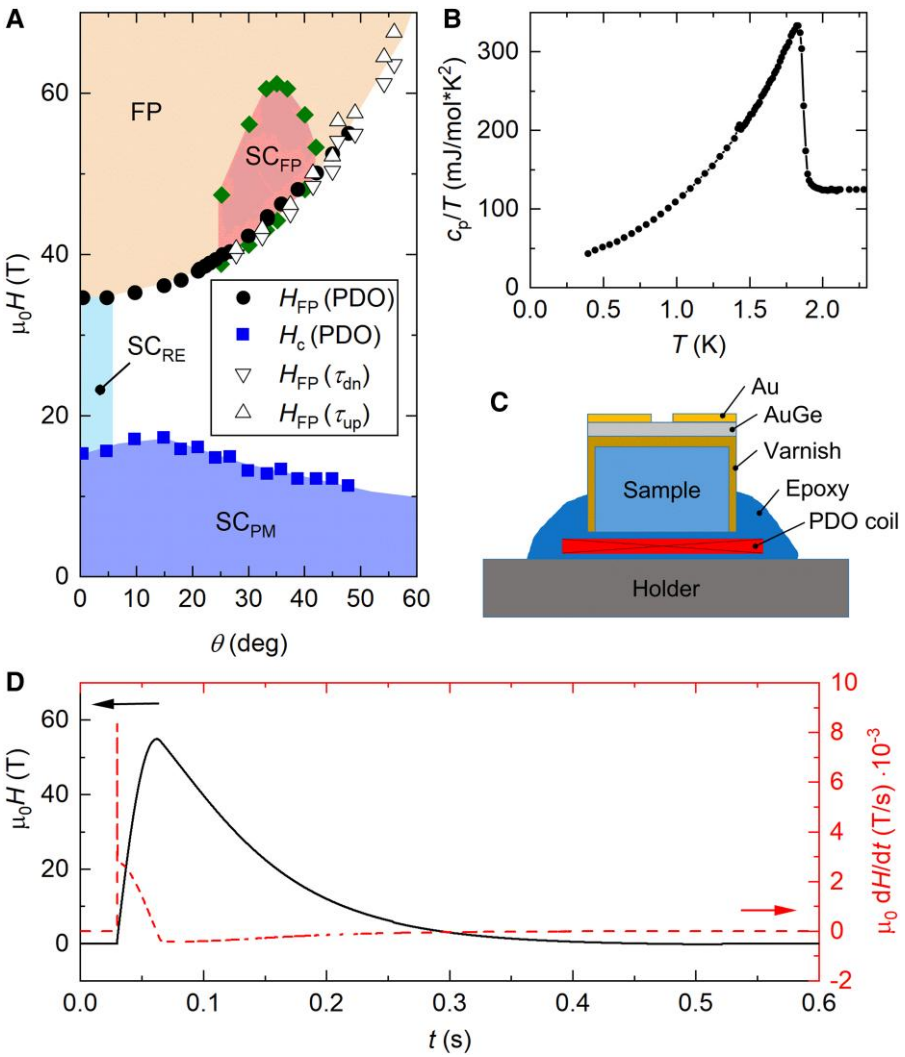

Fig. 1. A) Low-temperature field-angle ($H-\theta$) phase diagram of UTe $_2$, where $\theta = 0°$ corresponds to $H \parallel b$ and $\theta = 90°$ to $H \parallel c$. Solid squares mark the transition from the superconducting ground state (SC_{PM}) to the paramagnetic state or the reentrant superconducting state (SC_{SC_RE}) measured at $T \approx 0.6$K. Note that the region of the SC_{SC_RE} state is just roughly indicated to extend to $\theta \simeq 5°$. The solid circles and open triangles denote the first-order transition into the field-polarized paramagnetic state. Critical fields were obtained from PDO (solid circles, $T \approx 0.9$K) and torque $\tau_{up/dn}$ measurements (open triangles, for up-sweep and down-sweep, $T \approx 0.7$K) in this work. The solid triangles encircle the proposed high-field superconducting phase (SC_{SC_FP}); points were taken from Ran et al. (2). B) Specific heat vs. temperature for a single-crystal UTe_2 synthesized in the same batch as the ones used for MCE measurements. C) Schematic of the sample arrangements for simultaneous MCE and PDO measurements in pulsed fields. D) Magnetic field H (solid line) and dH/dt (dashed line) as a function of time for the pulsed magnet used in the MCE measurements.

temperature increase that is slightly less abrupt is seen in the MCE, followed by a temperature drop inside the SC_{FP} phase which, quite remarkably, retraces itself during the field down-sweep in an adiabatic fashion. The sample cooling continues upon crossing the phase boundary back into the paramagnetic normal state (The full angular dependence of the MCE vs. field is displayed and discussed in the Supplementary materials). Continuing along the down-sweep curves, the 33° PDO data show an increase in f due to the normal-to-SC_{PM} transition, accompanied by slight heating due to vortex motion revealed by the MCE data. The most significant results for $\theta = 33°$ are (i) the largely reversible change in temperature observed at H_m with minimal dissipative mechanisms. Here, a temperature increase on the up-sweep is suggestive of the opening of an energy gap for excitations. The drop in temperature during the down-sweep marks concomitantly the reversible closing of the gap. (ii) The retracing of the sample temperature inside the pink shadow region (up-sweep and down-sweep overlap) indicates adiabaticity, also compatible with a gaped state where superconducting pairs carry no entropy, decoupling the sample from the thermal bath.

We now turn to Fig. 3(A), which shows PDO frequencies for 15 angles in the range $0° \leq \theta \leq 48°$; as before, black curves signify rising H and red curves falling H. All traces here show that the field at which the frequency change associated with transitioning from the SC_{PM} phase (either into the SC_{RE} phase [$\theta \leq 10°$] or normal state [$\theta > 10°$]) occurs at lower fields on the field up-sweep creating loops, due to the heating seen in the MCE experiment. The sample is much closer to the bath temperature on the down-sweep, so that the corresponding step is at higher fields (25). Loops are also observed above H_m, for $24° \leq \theta \leq 42°$. While the critical field does not change (H_m is angle-dependent, yet temperature independent), the circuit inductance does, revealing strong MHz wave penetration in the up-sweep and screening in the field down-sweep. This is most likely caused by sample temperature difference between red and black curves, with black corresponding to high temperatures (above the SC_{FP} state critical temperature) and red corresponding to low temperatures.

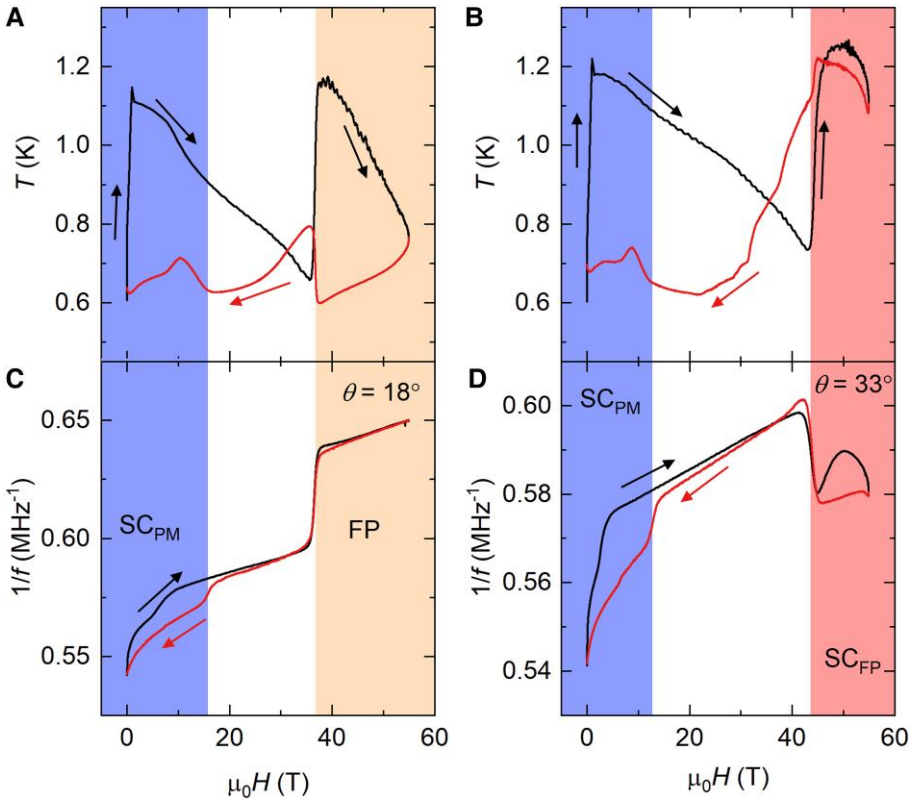

Fig. 2. A) Sample temperature T vs. field data for $\theta = 18°$. Data for the up-sweep (rising field) portion of the field pulse and those for the down-sweep are show with arrows indicating direction of field change. The background color indicates the superconducting and magnetic phases displayed in Fig. 1A. Note that the critical fields for the low-field superconducting state (vertical arrows) are marked for the down-sweep curves. B) T vs. H data for $\theta = 33°$. C and D) PDO data, shown as inverse frequency $1/f$, related to skin-depth (i.e. electrical resistance) in metals and penetration depth (caused by diamagnetic screening) in superconductors, vs. applied field, was recorded simultaneously with the thermal measurements shown in A and B). The color scheme is the same as in A and B).

Corresponding derivatives $(1/\mu_0)(df/dH)$ of the down-sweep data are shown in Fig. 3B. The critical fields H_c and H_{FP} shown in Fig. 1A were extracted from the extrema of this dataset. For the three lowest θ values (0, 5°, 10°), there is only a weak, broad feature between 15 and 20 T, reflecting that the transition is between two superconducting phases (SC_{PM} and SC_{RE}). For $\theta > 10°$, the weak feature is replaced by a well-defined minimum, as it now corresponds to a superconductor (SC_{PM})-to-normal transition.

The MCE measurements are summarized in Fig. 4; the increase in T in the SC_{FP} phase around $\theta = 33°$ clearly stands out, staying hot in the down-sweep data. This provides thermodynamic evidence that the sample becomes thermally decoupled from the bath (indeed, the SC_{FP} region does not change color for up-sweep and down-sweep, unlike the rest of the H, θ phase space), and a compelling proof for the bulk nature of the SC_{FP} state observed in UTe_2. On the other hand, due to the large heating effect caused by vortex motion at the onset of the magnet pulse, near $H = 0$, no clear phase boundary of the low-field superconducting phase can be identified in the up-sweep MCE data. Based on the PDO data (Fig. 3), the SC_{PM} phase is suppressed at a field of a few Tesla on the up-sweep. During the down-sweep, the phase boundary in the SC_{PM} phase coincides with the onset of gentle sample heating below ≈15 T and the corresponding upward step in the PDO data (Fig. 3).

Discussion

Before considering the thermodynamics of the onset of the high-field SC_{FP} state in more detail, it is worth considering alternative scenarios for the previous (nonthermodynamic) data used to identify the apparent superconductivity of this phase.

Indeed, one possibility might be a low (but nonzero) resistivity metallic phase caused by a field-induced Fermi-surface reconstruction at H_m that occurs over a restricted range of field orientations. A second candidate is a sliding density wave (sDW) that opens a gap in the material's excitations, causing thermal decoupling. These are truly exceptional cases at least equally, if not more, fascinating. Existing experimental data, however, provide a number of objections to such interpretations.

1. Hall-effect and thermopower measurements (3) for $H \parallel b$ indicate a very significant *decrease* in the charge-carrier density as one crosses H_m into the FP (normal) state, leading to a strong *increase* in the resistivity (2, 3). On the other hand, PDO data show a significantly different change in electrical properties (i.e. over a restricted range of θ). If the changes were due to a large *increase* in carrier density and/or mobility (good metal, yet not superconducting), one would expect that the metamagnetic transition would also change the character for these angles. However, torque magnetometry data (Fig. 5) carried out over a wide range of field orientations show that the position and size of the magnetization jump at H_m vary smoothly and monotonically with θ. Signs of superconductivity in the torque data are, however, too small to detect due to the magnetic signal background.
2. An increase in the charge-carrier density at H_m (such as due to the closing of an energy gap) leads to cooling (see Refs. (26, 27) for $Ce_3Bi_4Pt_3$ and Ref. (23) for URu_2Si_2) of the sample

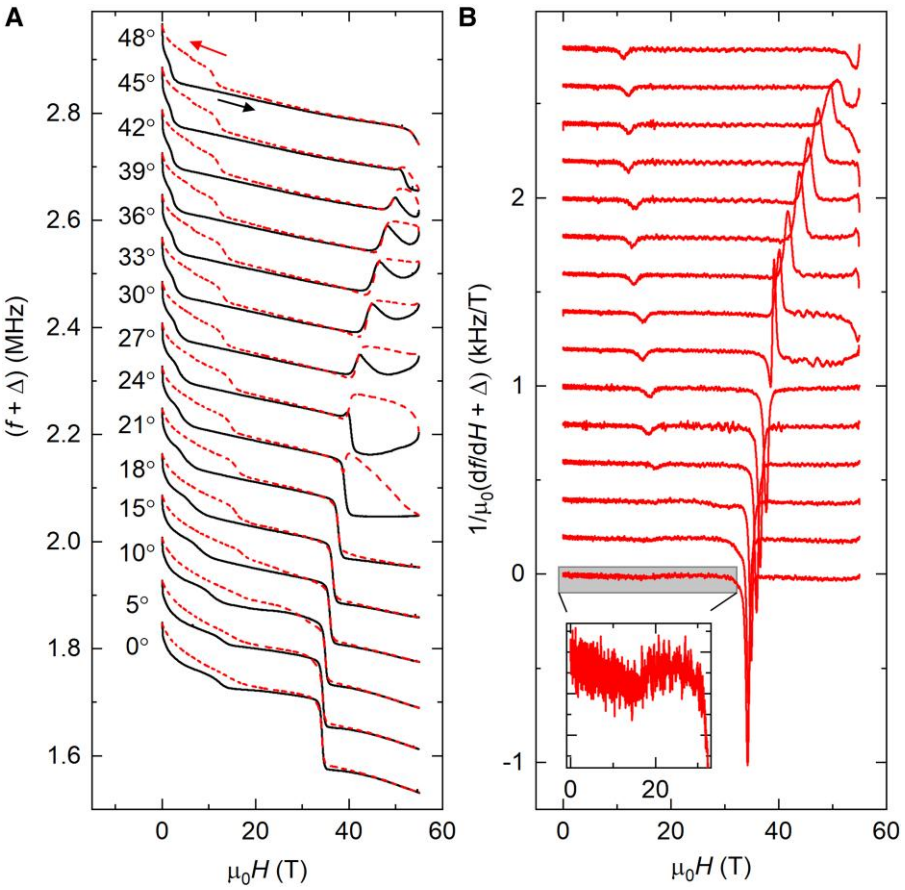

Fig. 3. A) PDO frequency (a proxy for electrical conductivity) vs. magnetic field for different angles θ displayed on the left of each curve. The field up-sweep and down-sweep are shown as solid and dashed curves, respectively. The smooth change in frequency with field (slope) observed in the data is often seen when the field is applied perpendicular to the flat PDO detection coils (21). B) Derivative of the down-sweep curves shown in A). The inset shows a low-field feature indicating the transition between the SC_{PM} and SC_{RE} superconducting states close to $\theta = 0$. Curves in A) and B) are shifted vertically by an offset Δ for clarity.

during the field up-sweep and heating in the down-sweep, which is incompatible with the data in this report. A highly conductive field-induced gapless metallic state would also likely lead to eddy-current heating in changing fields of both directions, which is not present in the high-field MCE data.

3. The observation of reversible heating/cooling upon entering/exciting the high-field SC_{FP} phase is indicative of the opening/closing of an energy gap in excitations. This is, moreover, accompanied by sample thermal decoupling (sudden adiabaticity), i.e. an abrupt increase in the sample thermal relaxation time constant $\tau \propto C/K$, where C is the sample heat capacity and K is its thermal conductance. Thermal decoupling is a characteristic of the superconducting state in materials where heat is transported by charge carriers. Numerous related U-based compounds, such as UBe_{13}, UPt_3, UCoGe, and URhGe (28–34), as well as in UTe_2 in low fields (8), show a reduced thermal conductivity in the superconducting state. In the case of UCoGe, a 2- to 5-fold increase in the thermal relaxation time constant can be estimated in the superconducting state. Such an increase can explain our pulsed-field MCE data in UTe_2, where we estimate the time constant to be at least $\tau_{SC} \geq 26$ ms and substantially longer than the experiment time scale of 8 ms above 45 T (see Fig. 1D).
4. We note that an sDW scenario, characterized by an energy gap and low electrical resistance, is an unlikely candidate for the field-induced state in UTe_2. The reason is that density waves in real materials are pinned by defects and impurities, often requiring a large applied electric field to "slide" in a frictionless fashion (35). So, while the thermodynamic signature of a density wave should in principle be present in the MCE data, it will be accompanied by an increase in electrical resistance due to pinning, which is incompatible with our observation of strongly reduced penetration depth and rules out such scenario.
5. The PDO data used to detect the SC_{FP} state in Ran et al. (2) (and those in this paper) behave in a qualitatively similar manner to PDO measurements on more conventional superconductors such as pnictides (25, 36) and cuprates (37), especially in the hysteresis observed between up-sweeps and down-sweeps of the field. In contrast, PDO data measured in systems where there is a large field-induced increase in carrier density but no superconductivity (38, 39) behave in a very different way, e.g. showing different hysteretic characteristics.
6. The typical energy scales associated with the transition at H_m are ~40 K (see Introduction). Any phenomenon associated with increased (normal-state) conductivity due to a Fermi-surface change at H_m would be expected to persist (or slowly die away) over a temperature range similar to this. In contrast, the upper-temperature limit of the SC_{FP} phase is about 1.9 K (2), very similar to the critical temperatures of the SC_{PM} and

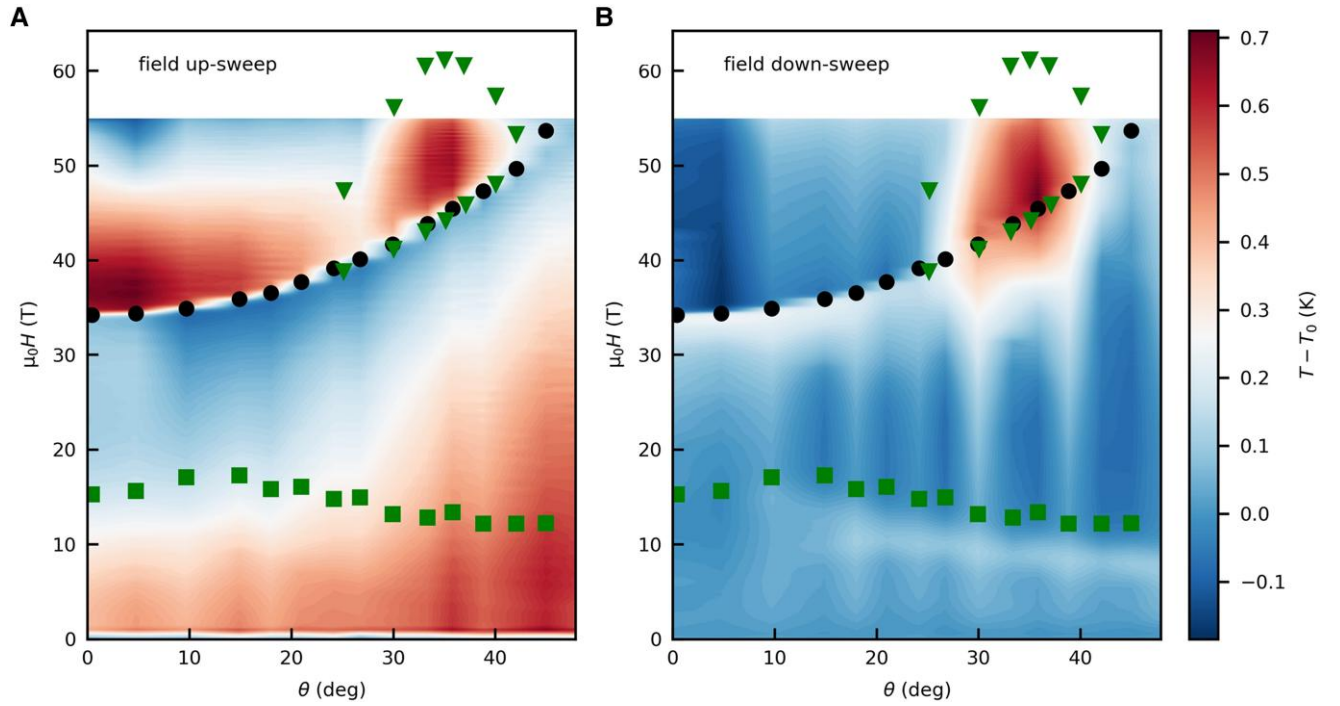

Fig. 4. Contour plot of the sample temperature T as a function of the angle θ at which the magnetic field H is applied for the up-sweep A) and down-sweep B). The black circles indicate the metamagnetic phase transitions discussed in the text, green squares and triangles enveloping the high-field superconducting state were taken from Ran et al. (2). The reversible temperature increase and adiabaticity observed for $H > 40$ T and $30° < \theta < 40°$, quite distinct from results at all other angles and fields, coupled with high electrical conductivity, are together consistent with a field-induced superconducting state in UTe_2. The initial temperature before the field pulses is $T_0 \sim (0.6 \pm 0.1)$K, variations in T_0 cause vertical stripes to appear in both contour plots.

SC_{RE} superconducting phases (7), suggesting a common or closely related origin.

In view of the above points, the following discussion of the thermodynamics occurring at and around H_m assumes that the SC_{FP} phase is superconducting.

As shown in a previous study (20) for $H \parallel b$, the metamagnetic transition at H_m is first order at low temperatures and accompanied by hysteresis losses. In the current, field-orientation-dependent study, the temperature change ΔT_{FP} observed at H_m can be described as follows (see Fig. 6). (i) During the up-sweep, ΔT_{FP} is positive and decreases with increasing θ (dashed line in Fig. 6B). (ii) ΔT_{FP} increases for θ between 25° and 35° as the sample transitions into the SC_{FP} state. (iii) ΔT_{FP} decreases with θ once again when the SC_{FP} state is suppressed at larger θ. During the down-sweep of the field, ΔT_{FP} (Fig. 6B, red points) is always smaller than that during the up-sweep. For the falling field, ΔT_{FP} is positive for $\theta < 27°$ and becomes negative for larger angles.

In making a quantitative description of the thermodynamics of the metamagnetic transition, we assume that the overall entropy change is a sum of reversible and irreversible processes,

$$\Delta S = \Delta S_{rev} + \Delta S_{irr} = \frac{C_p \Delta T}{T} + \frac{\partial Q_{loss}}{T}, \quad (1)$$

where ΔS_{rev} is the latent heat released during the transition, which is recovered when the field crosses H_m in the opposite sense, and C_P is the heat capacity at constant pressure. The small field width of the metamagnetic transition leads us to assume adiabatic conditions and extract the temperature change ΔT directly from the magnetocaloric measurements. The time to cross the transition at H_m is ~0.6 ms—significantly shorter than the thermal relaxation timescale τ of the sample in the FP state which is around 10ms for our equipment. τ was estimated from the $T(t)$ behavior above H_m (Fig. 6A), yet it is at least 3× longer in the SC_{FP} region of the phase diagram (based on the fact that the sample temperature does not change much during the extent of the high field portion of the sweep). We obtain the reversible temperature changes at the metamagnetic transition through $\Delta T_{rev} = (\Delta T_{FPup} - \Delta T_{FPdown})/2$, where the subscripts "up" and "down" refer to the up-sweep and down-sweep of the field, respectively. On the other hand, irreversible processes such as Joule heating contribute to the temperature change in both field-sweep directions, and therefore, $\Delta T_{irr} = (\Delta T_{FPup} + \Delta T_{FPdown})/2$.

Using that $C_p/T \approx 250$ mJ mol^{-1} K^{-2} and assuming that C_p shows weak temperature dependence below 2K at 35T (8, 20), for $\theta < 25°$ we obtain an almost constant value, $\Delta S_{rev} \approx 30$ mJ mol^{-1} K^{-1}. Within the SC_{FP} phase, ΔS_{rev} increases, peaking at $\Delta S_{rev} \approx 80$ mJ mol^{-1} K^{-1} close to $\theta = 35°$ (Fig. 6C).[b] Therefore, entering the SC_{FP} phase releases at least an additional ≈50 mJ mol^{-1} K^{-1} in latent heat. Assuming (as justified above) that the SC_{FP} represents a field-induced superconducting state, the estimated additional latent heat is likely to result from the formation of a gap at the Fermi energy and an entropy reduction due to pair condensation (7).

The irreversible component ΔS_{irr} mainly consists of hysteretic losses during the first-order metamagnetic transition and, bearing in mind the similarity of the behavior of the PDO data in the SC_{FP} state to that in the SC_{PM} phase (see also Ran et al. (2)), what is likely to be dissipation due to vortex movement. As shown in Fig. 6D, rotating H to higher θ leads to an overall decrease in ΔS_{irr}, apart from a small local uptick around $\theta = 35°$. As this is roughly in the middle of the θ range over which the SC_{FP} phase occurs, it possibly coincides with dissipation caused by a combination of metamagnetism, some vortex motion, and lack of perfect adiabaticity. Note that while H_m increases with increasing θ, the jump in the

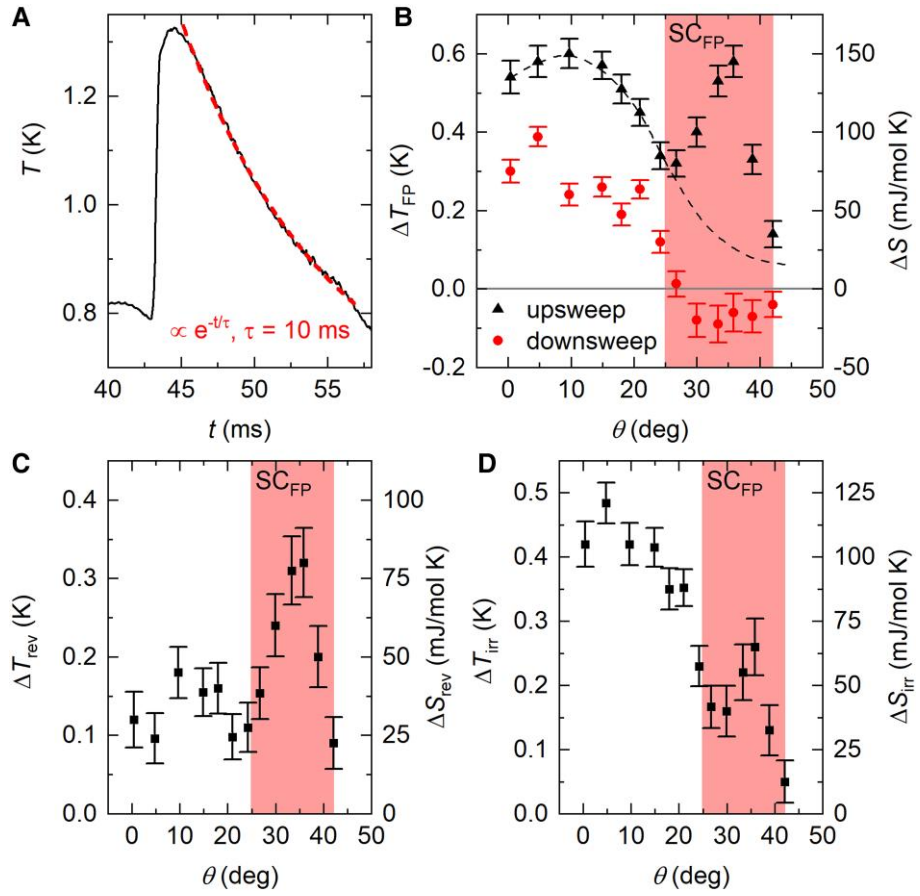

Fig. 5. Metamagnetic transition in UTe_2 as seen in the magnetic torque signal measured at different angles at $T = (0.7 \pm 0.1)$K. Up-sweep and down-sweep of the magnetic field are indicated by arrows. In general, the curve with the higher transition field corresponds to the up-sweep.

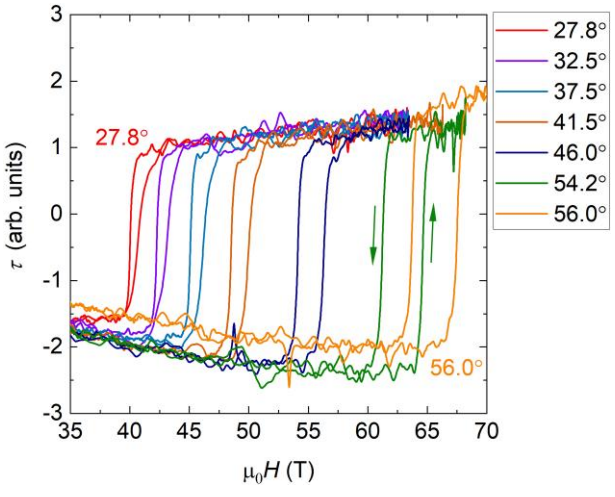

Fig. 6. A) Temperature vs. time during the up-sweep of the magnetic field pulse for $H \parallel b$. The time frame shows the metamagnetic transition and the subsequent relaxation back to the bath temperature, which is approximated by an exponential decay (dashed line). B) Temperature change $\Delta T_{FP}(\theta)$ at the metamagnetic transition during the up-sweep (solid triangles) and down-sweep (solid circles) of the magnetic field. C) Reversible and D) irreversible component of ΔT_{FP} as a function of the angle θ (left axes). While reversible processes are prevalent in the SC_{FP} phase at $\theta \simeq 33°$, irreversible mechanisms or dissipation dominate in the small θ region. The corresponding entropy changes are shown on the right axes of each figure.

magnetization at H_m at 1.4K does not change significantly between $H \parallel b$ and $H \parallel [011]$ (40). Torque measurements shown in Fig. 5 also vary smoothly as a function of angle. Therefore, it is unlikely that the small irreversible heat involved when entering the SC_{FP} phase is of magnetic origin. Similarly, it is unlikely that the changes in PDO data between the FP and SC_{FP} phases are due to change of magnetic permeability between different magnetic states.

Finally, we remark that the boundaries between the various low-temperature and high magnetic field phases of UTe_2 derived in this work from PDO and MCE data match with those for chemical vapor transport (CVT)-grown samples in the literature (2, 7) very closely. This is of interest because the zero- or low-field behavior of UTe_2 seems very sensitive to the source, growth method, and quality of the crystals used (an excellent summary is given in Aoki et al. (7)). The present study employs crystals from different sources to those used to produce the phase diagrams reported in Refs. (2, 7), perhaps suggesting that the high magnetic field properties of UTe_2 are less sensitive to sample-dependent disorder than those in zero or small magnetic fields (41, 42).

Conclusion

The simultaneous zero-electric current MCE, MHz conductivity measurements, and angular-dependent torque magnetometry are carried out on single crystals of UTe_2 as a function of magnetic field magnitude and orientation, using pulsed magnetic fields of

up to 55 T. A pronounced and fully reversible magnetocaloric effect characteristic of a thermally decoupled (adiabatic) state is observed close to the metamagnetic transition into the proposed high-field SC_{FP} phase. This amounts to compelling evidence for the stabilization of a field-induced energy-gaped state of concurrent high electrical and poor thermal conductivity, i.e. the first thermodynamic evidence that the SC_{FP} state represents a field-stabilized bulk superconducting phase of UTe_2. The sudden increase in thermal relaxation time constant required to explain our results is in line with observations in other U-based magnetic superconductors where a reduction in thermal conductivity and enhancement of specific heat is observed for temperatures in the $T_c/2$ range. A nodal superconducting order parameter implies the presence of entropy-carrying quasiparticles that contribute to both, the thermal conductivity and the material's heat capacity, and it is a priori difficult to say which of these effects have a larger impact on the thermal relaxation time. A more definitive statement on the symmetry of the order parameter requires complementary experimental efforts, accompanied by theoretical modeling. Last but not least, though the corresponding features in the PDO and MCE data are weak, there are distinct indications of the boundary between the SC_{PM} and SC_{RE} phases. This seems to confirm that though both states are superconducting, they are distinct phases with subtly different properties (7, 8).

Materials and methods

Sample characterization

Single crystals of UTe $_2$ are grown using chemical vapor transport; the conditions are the same as for sample s4 described in Rosa et al. (43), where further details can be found. To provide initial characterization prior to the pulsed-field experiments, heat-capacity measurements are performed using a commercial calorimeter that utilizes a quasiadiabatic thermal relaxation technique. In addition, the electrical resistivity ρ is characterized using a standard four-probe configuration with an AC resistance bridge. Resistivity (not shown) and heat-capacity measurements on crystals from this batch show a single sharp transition around 1.9K (Fig. 1B).

Magnetocaloric measurements

Figure 1C shows a schematic drawing of the sample environment for the pulsed-field experiments. The pancake coil for the PDO measurements (10 turns of insulated 50-gauge copper wire) is sandwiched between a G10 holder and the single-crystal UTe_2 sample. The sample was coated with a thin film of GE varnish to avoid electrical contact with the layers above. The MCE thermometer is ≈100-nm thick semiconducting AuGe film (16at% Au) deposited directly on the varnish-coated sample to ensure good thermal coupling between the sample and film. To improve the contact resistance, Au pads are deposited on the AuGe film. The AuGe film is calibrated against a commercial Cernox sensor; film resistances range from 6Ω at room temperature to 250Ω at 0.6K. The sample is glued to the holder with Stycast epoxy to prevent any sample movement due to the large magnetic torque when the field is aligned close to the *b*-axis.

PDO measurements

The PDO measurements employ equipment similar to that described in Refs. (21, 22, 25, 36, 38, 39); the technique is well established for mapping the irreversibility and upper critical fields of superconductors in pulsed magnetic fields (25, 36). The magnetocaloric and PDO experiments were performed in the NHMFL's mid-pulse magnet, which provides a peak magnetic field of 55T with a rise time of ≈ 30ms and a total pulse duration of 500ms. A typical field pulse and its derivative are shown in Fig. 1D. The sample holder was fixed to the rotating platform of a cryogenic goniometer (44) placed within a ^{3}He cryostat. The sample was immersed in liquid ^{3}He at a bath temperature of 0.6 ± 0.1 K during the field pulses.

Torque measurements

Additionally, we conducted piezo torque magnetometry measurements in pulsed magnetic fields up to 75T by using membrane-type surface-stress sensors at the NHMFL at LANL with a high-frequency (≈300 kHz) AC excitation current of ≈500 μA. The angular-dependent torque measurements were performed at 0.7K with the sample immersed in liquid ^{3}He. In the experiments, we used a balanced Wheatstone bridge between the piezoresistive pathways. Crystals were mounted with the *b*-axis perpendicular to the cantilever plane.

Notes

[a] In the PDO circuit, the resonant frequency $f = 1/\sqrt{LC}$, where L is the circuit inductance and C is the capacitance. The inductance of a solenoid of N turns, area A, and length l is $L = \mu N^2 A/l$, where μ is the permeability of the core material. Due to the alternate current (AC) skin-depth effect in metallic samples of low resistance, the effective volume, and hence inductance, of the coil is reduced. Hence, $\Delta f \propto (\Delta\rho)^{-1}$. In superconducting samples, instead, the change in resonance frequency is driven by changes in superconducting penetration depth and hence related to direct current (DC) magnetic field screening.

[b] We note a discrepancy in the entropy change at the metamagnetic transition between the present results and the values reported in the brief report by Imajo et al. (20). The difference is likely related to the conditions in the present work, i.e. a stronger link to the thermal bath needed to reach lower ^{3}He temperatures leading to the quasiadiabatic magnetization of the sample. The difference does not affect the conclusions of the current paper.

Acknowledgments

The authors thank M. Lee, L. Civale, and A. Shehter for insightful discussions.

Supplementary Material

Supplementary material is available at *PNAS Nexus* online.

Funding

A portion of this work was performed at the National High Magnetic Field Laboratory, which is supported by the NSF Cooperative Agreement No. DMR-1644779, the US DOE and the State of Florida. This material is based upon work supported by the US Department of Energy, Office of Science, National Quantum Information Science Research Centers. S.M.T. acknowledges support from the Los Alamos Laboratory Directed Research and Development Program through project 20210064DR. J.S. and M.J. thank the DoE BES FWP "Science of 100 T" for support in developing techniques

used in these experiments. R.S., Y.L., and M.J. acknowledge support by the NHMFL UCGP program and the G. T. Seaborg Institute Postdoctoral Fellow Program under project number 20210527CR.

Author Contributions

R.S., P.F.S.R., S.M.T., and M.J. conceived the idea. R.S. and E.L.B. ran the MCE experiments. R.S. and J.S. performed the PDO measurements. Y.L. and D.N.N. ran the torque magnetometry experiment. P.F.S.R. and S.M.T. provided the single-crystal samples. R.S., J.S., B.M., and M.J. wrote the manuscript. All coauthors contributed to the discussion.

Preprints

This manuscript was posted on a preprint: https://doi.org/10.48550/arXiv.2206.06508.

Data Availability

The data in this study are available upon reasonable request to the corresponding authors R.S. and M.J.

References

1 Ran S, *et al.* 2019. Nearly ferromagnetic spin-triplet superconductivity. *Science*. 365(6454):684–687.
2 Ran S, *et al.* 2019. Extreme magnetic field-boosted superconductivity. *Nat Phys*. 15(12):1250–1254.
3 Knafo W, *et al.* 2019. Magnetic-field-induced phenomena in the paramagnetic superconductor UTe_2. *J Phys Soc Jpn*. 88(6):063705.
4 Knebel G, *et al.* 2019. Field-reentrant superconductivity close to a metamagnetic transition in the heavy-fermion superconductor UTe_2. *J Phys Soc Jpn*. 88(6):063707.
5 Nakamine G, *et al.* 2019. Superconducting properties of heavy fermion UTe_2 revealed by ^{125}Te-nuclear magnetic resonance. *J Phys Soc Jpn*. 88(11):113703.
6 Jiao L, *et al.* 2020. Chiral superconductivity in heavy-fermion metal UTe_2. *Nature*. 579:523–527.
7 Aoki D, *et al.* 2022. Unconventional superconductivity in UTe_2. *J Phys Condens Matter*. 34(24):243002.
8 Rosuel A, *et al.* 2023. Field-induced tuning of the pairing state in a superconductor. *Phys Rev X*. 13:011022.
9 Matsumura H, *et al.* 2023. Large reduction in the *a*-axis knight shift on UTe_2 with $T_c = 2.1$ K. *J Phys Soc Jpn*. 92:063701.
10 Sundar S, *et al.* 2019. Coexistence of ferromagnetic fluctuations and superconductivity in the actinide superconductor UTe_2. *Phys Rev B*. 100(14):140502(R).
11 Paulsen C, *et al.* 2021. Anomalous anisotropy of the lower critical field and Meissner effect in UTe_2. *Phys Rev B*. 103(18):L180501.
12 Duan C, *et al.* 2020. Incommensurate spin fluctuations in the spin-triplet superconductor candidate UTe_2. *Phys Rev Lett*. 125(23):237003.
13 Thomas SM, *et al.* 2020. Evidence for a pressure-induced antiferromagnetic quantum critical point in intermediate-valence UTe_2. *Sci Adv*. 6(42):eabc8709.
14 Aoki D, *et al.* 2020. Multiple superconducting phases and unusual enhancement of the upper critical field in UTe_2. *J Phys Soc Jpn*. 89(5):053705.
15 Miyake A, *et al.* 2019. Metamagnetic transition in heavy fermion superconductor UTe_2. *J Phys Soc Jpn*. 88(6):063706.
16 Miyake A, *et al.* 2022. Magnetovolume effect on the first-order metamagnetic transition in UTe_2. *J Phys Soc Jpn*. 91(6):063703.
17 Niu Q, *et al.* 2020. Evidence of Fermi surface reconstruction at the metamagnetic transition of the strongly correlated superconductor UTe_2. *Phys Rev Res*. 2(3):033179.
18 Knafo W, *et al.* 2021. Comparison of two superconducting phases induced by a magnetic field in UTe_2. *Commun Phys*. 4(1):40.
19 Helm T, *et al.* 2023. Field-induced compensation of magnetic exchange as the origin of superconductivity above 40 T in UTe_2. https://arxiv.org/abs/2207.08261.
20 Imajo S, *et al.* 2019. Thermodynamic investigation of metamagnetism in pulsed high magnetic fields on heavy fermion superconductor UTe_2. *J Phys Soc Jpn*. 88(8):083705.
21 Altarawneh MM, Mielke CH, Brooks JS. 2009. Proximity detector circuits: an alternative to tunnel diode oscillators for contactless measurements in pulsed magnetic field environments. *Rev Sci Instrum*. 80(6):066104.
22 Ghannadzadeh S, *et al.* 2011. Measurement of magnetic susceptibility in pulsed magnetic fields using a proximity detector oscillator. *Rev Sci Instrum*. 82(11):113902.
23 Jaime M, Kim KH, Jorge G, McCall S, Mydosh JA. 2002. High magnetic field studies of the hidden order transition in URu_2Si_2. *Phys Rev Lett*. 89(28):287201.
24 Silhanek AV, *et al.* 2006. Irreversible dynamics of the phase boundary in $U(Ru_{0.96}Rh_{0.04})_2Si_2$ and implications for ordering. *Phys Rev Lett*. 96(13):136403.
25 Smylie MP, *et al.* 2019. Anisotropic upper critical field of pristine and proton-irradiated single crystals of the magnetically ordered superconductor $RbEuFe_4As_4$. *Phys Rev B*. 100:054507.
26 Jaime M, *et al.* 2000. Closing the spin gap in the Kondo insulator $Ce_3Bi_4Pt_3$ at high magnetic fields. *Nature*. 405:160–163.
27 Jaime M. 2010. Frontiers of condensed matter physics explored with high-field specific heat. *Netsu Sokutei*. 37:26–33.
28 Ravex A, Flouquet J, Tholence JL, Jaccard D, Meyer A. 1987. Thermal conductivity and specific heat measurements on UBe_{13}. *J Magn Magn Mater*. 63–64:400–402.
29 Suderow H, Brison JP, Huxley A, Flouquet J. 1997. Thermal conductivity and gap structure of the superconducting phases of UPt_3. *J Low Temp Phys*. 108:11–30.
30 Hagmusa IH, *et al.* 2000. Magnetic specific heat of a urhge single crystal. *Physica B*. 281–282:223–225.
31 Prokeš K, *et al.* 2002. Electronic properties of a URhGe single crystal. *Physica B*. 311:220–232.
32 Howald L. 2006. Interactions entre la supraconductivité et la criticité quantique, dans les composes $CeCoIn_5$, URhGe et UCoGe [PhD thesis]. [Grenoble, France]: Université de Grenoble.
33 Howald L, Taupin M, Aoki D. 2014. Multigap superconductivity in the ferromagnetic superconductor UCoGe revealed by thermal conductivity measurements. *Phys Res Int*. 2014:54939.
34 Taupin M, Howald L, Aoki D, Brison J-P. 2014. Superconducting gap of UCoGe probed by thermal transport. *Phys Rev B*. 90:180501.
35 Stokes JP, Bloch AN, Janossy A, Gruner G. 1984. Thermoelectric aspects of charge-density-wave transport in TAs_3. *Phys Rev Lett*. 52:372–375.
36 Nikolo M, *et al.* 2018. Upper critical and irreversibility fields in Ni- and Co-doped pnictide bulk superconductors. *Physica B: Condens Matter*. 536:833–838.
37 Singleton J, *et al.* 2010. Magnetic quantum oscillations in $YBa_2Cu_3O_{6.61}$ and $YBa_2Cu_3O_{6.69}$ in fields of up to 85 T: patching the hole in the roof of the superconducting dome. *Phys Rev Lett*. 104:086403.
38 Xiang Z, *et al.* 2021. Unusual high-field metal in a Kondo insulator. *Nat Phys*. 17(7):788–793.

39 Götze K, *et al.* 2020. Unusual phase boundary of the magnetic-field-tuned valence transition in $CeOs_4Sb_{12}$. *Phys Rev B*. 101: 075102.
40 Miyake A, *et al.* 2021. Enhancement and discontinuity of effective mass through the first-order metamagnetic transition in UTe_2. *J Phys Soc Jpn*. 90(10):103702.
41 Wu Z, *et al.* 2023. Enhanced triplet superconductivity in next-generation ultraclean UTe_2. https://arxiv.org/abs/2305.19033.
42 Frank CE, *et al.* 2023. Orphan high field superconductivity in non-superconducting uranium ditelluride. https://arxiv.org/abs/2304.12392.
43 Rosa PFS, *et al.* 2022. Single thermodynamic transition at 2 K in superconducting UTe_2 single crystals. *Commun Mater*. 3:33.
44 Willis X, Ding X, Singleton J, Balakirev FF. 2020. Cryogenic goniometer for measurements in pulsed magnetic fields fabricated via additive manufacturing technique. *Rev Sci Instrum*. 91(3):036102.